scientific data

OPEN

DATA DESCRIPTOR

Dislocation-Grain Boundary Interaction Dataset for FCC Cu

Khanh Dang[1], Sumit Suresh[2], Avanish Mishra[3], Ian Chesser[4], Nithin Mathew[3], Edward M. Kober[3] & Saryu Fensin[2] ✉

Interactions between dislocations and grain boundaries play a major role in controlling the strength and ductility of structural materials. Experimentally, assessing and probing geometric and stress-based criteria at the local level for dislocation transmission through grain boundaries remains challenging. Therefore, there have been many efforts to systematically generate datasets of dislocation-grain boundary interactions (DGI) via computational models such as molecular dynamics simulations. So far, most DGI datasets have focused only on the subset of nominal minimum-energy grain boundary structures, which limits their applicability, especially to materials processed far from equilibrium. We present a comprehensive database of dislocation-grain boundary interactions for edge, screw, and 60° mixed dislocation with 330 <110> and 257 <112> symmetric tilt grain boundaries (total of 587) in FCC Cu consisting of 73 minimum-energy grain boundary structures and 514 metastable structures. The dataset contains the outcomes for 5234 unique interactions for various dislocation types, grain boundary structures, and applied shear stresses.

Background & Summary

Designing structural alloys with both high strength and excellent ductility remains one of the grand challenges in materials science and engineering. One strategy that has proven effective in certain alloys is known as grain boundary (GB) engineering, which involves manipulating the GB network via the introduction of high densities of specific GBs such as coherent twin boundaries[1–3]. At the core of this strategy is the role that GB structure plays in determining the outcome of dislocation-GB interactions (DGI). For a similar applied stress state, some boundaries may block or absorb dislocations, leading to strain localization, while other boundaries promote transmission. As a result, the DGIs alter the strength and ductility of a material depending on the volume fraction of boundary types in the material[4–6].

Macroscopically, the Hall-Petch relationship hypothesizes that material strength can be increased by decreasing the grain size due to an enhanced effect of dislocation blockage (which we refer to as pinning) as the density of GBs is increased[7]. This relationship captures the effects of average grain size on yield strength without considering local GB structure. There are many situations where local GB structure impacts mechanical behavior, especially far from equilibrium. For instance, Fensin *et al*. showed that only certain boundaries can avoid void nucleation under shock loading by dissipating stress through plastic deformation[8]. Simulations and experiments of irradiated metals demonstrate that non-equilibrium GB structures may have a higher sink efficiency than well-annealed GBs[9,10]. Other examples of the impact of GB metastability on mechanical behavior can be found in a recent review[11].

For DGI, the role of GB structure on the dislocation transmissibility remains unknown despite many experimental, theoretical, and computational efforts over the past few decades. Microscopic geometric and stress criteria for dislocation transmission through grain boundaries, such as minimizing the angle between the intersection lines of the incoming and outgoing dislocations or maximizing the resolved shear stress on the outgoing slip system, have been proposed and experimentally validated[6]. One of the commonly utilized geometric parameters for examining slip or dislocation transmission across GB is m', which assesses the slip system degree of coplanarity[12]. However, similar to the Hall-Petch relationship, these criteria fail to capture the role of GB structure and the local atomic arrangement on GB-dislocation interactions.

[1]Materials Science and Technology Division, Los Alamos National Laboratory, Los Alamos, New Mexico, 87544, USA. [2]Materials Physics and Applications Division, Los Alamos National Laboratory, Los Alamos, New Mexico, 87544, USA. [3]Theoretical Division, Los Alamos National Laboratory, Los Alamos, New Mexico, 87544, USA. [4]X Computational Physics Division, Los Alamos National Laboratory, Los Alamos, New Mexico, 87544, USA. ✉e-mail: saryuj@lanl.gov

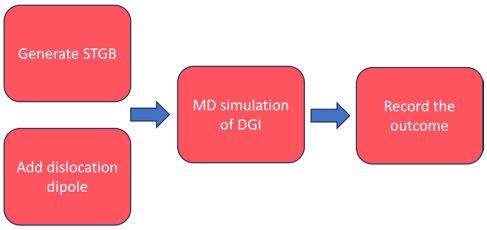

Fig. 1 Workflow to generate the DGI database.

The lack of high-fidelity DGI datasets with details about dislocation type, applied stress, and, most importantly, diverse GB structures, inhibits our ability to construct more accurate models for GB-dislocation interactions. Experimentally, it remains challenging to systematically and efficiently generate these datasets. Computationally, most DGI datasets are limited in the number of data points since these have previously focused only on a subset of grain boundary structures or dislocation types[13–18]. For instance, Cheng *et al.*[13] studied the interactions between edge dislocations and [110] symmetric tilt grain boundaries (STGBs) such as Σ3(112), Σ9(114), and Σ9(221) in W. While this study found that the DGIs depend on the grain boundary structure and the exact location of the interaction within the grain boundary, it was challenging to propose a new criterion for slip transmission due to limited data. Moreover, it is unfeasible to merge different DGI datasets into a comprehensive one since boundary conditions usually vary and significantly affect the simulation results[19]. Recent efforts to generate large datasets of GB structures by atomistic simulations have served as foundations to further drive the research in DGI[20–22]. For example, one of the most cited datasets of computed GB structures and properties is by Olmsted *et al.*[20]. This dataset contains 388 unique minimum-energy GB structures of Ni and Al and their corresponding energies. A subset of this dataset (33 different FCC Ni bicrystals) was utilized for a DGI study[18]. It was found that the minimum residual Burgers vector and the disorientation angle between the two grains are strong indicators of DGI transmissibility. However, the GB structures in these previous studies were simplified by choosing the minimum energy configurations, which are not necessarily observed in experiments. It was shown recently that metastable GB structures (i.e., those which have higher energies than the minimum configuration) can alter the outcome of the DGI[23,24]. Therefore, there is a need for a consistent and comprehensive dataset that explores DGI as a function of dislocation character and GB atomic structure.

The goal of this work is to fill this gap by establishing a comprehensive database of DGI in Cu as a model FCC material. While the trends for the DGI dataset are expected to vary for different material systems, the approach described in this work can be adapted for other material systems (especially those with FCC crystal structures). MD simulations of DGI are systematically performed for different type of dislocations (edge, screw, and mixed 60°), GB structures (330<110>and 257<112> symmetric tilt GBs with many metastable structures), and applied stresses (250, 500, and 750 MPa). Altogether, this database includes 5234 unique dislocation - GB interactions, which is the most of its kind currently. This comprehensive DGI database is expected to be useful to train AI/ML models to predict DGI as a function of GB structure, dislocation type, and applied stress.

Methods

Workflow overview. The data and simulation workflow used to characterize and obtain DGI via MD simulations consists of three steps as shown in Fig. 1: (i) First, GB structures (including metastable states) are generated using the standard γ-surface approach[22,25]. Dislocation dipoles are constructed using the displacement field of an infinitely long dislocation dipole[26]. Both types of defects are generated via LAMMPS input scripts. (ii) Second, dislocations are driven into the GBs under an applied stress[19]. The DGI outcomes are recorded and indexed into a database. Details about the database, such as the parameters needed to reproduce GB structures as well as DGI results, are described in the Data Records section. Each step in the workflow is described in more detail below.

Dislocation-grain boundary interactions via molecular dynamics simulations. All dislocation-grain boundary interactions in Cu are performed via the open-source simulation software Large-scale Atomic/Molecular Massively Parallel Simulator (LAMMPS)[27]. The atomic interactions between Cu atoms were modeled using an Embedded Atom Method (EAM) interatomic potential developed by Mishin *et al.*[28]. This interatomic potential can accurately reproduce GB and dislocation core structures as well as their corresponding energies[28]. Therefore, it has been widely used in DGI studies[23,29,30]. The simulation results are manually recorded by analyzing atomic snapshots before and after the interaction via the visualization software OVITO and the dislocation extraction algorithm (DXA)[31]. Simulation details about (i) the construction of the GB structure, (ii) the DGI simulation setup, and (iii) the determination of the geometrical criteria (m') are discussed in greater details below.

Grain boundary structures and energies. Figure 2 shows the simulation setup to generate the dataset. Both <110> and <112> STGBs are generated using the γ-surface approach[22,25]. The X direction is always oriented along the tilt axes, and the Y direction is normal to the GB plane (which can be found in the database for all interactions). Periodic boundary conditions are applied in all three directions to allow for complete control of the stress state. This simulation setup has been demonstrated to be efficient for DGI in previous work[19]. For the

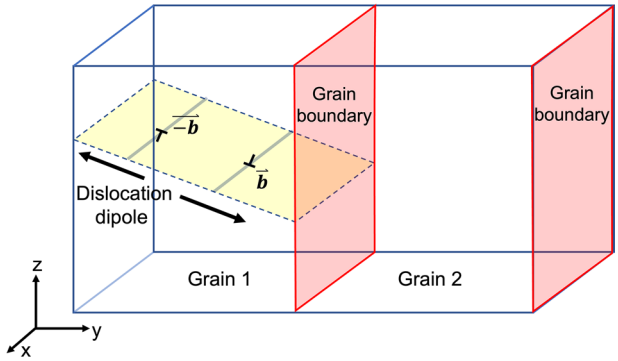

Fig. 2 Simulation setup with a bicrystal composed of two symmetric tilt GBs (<112> or <110>). An infinitely long dislocation dipole with edge, screw and mixed (60°) character angles is generated in grain 1 using a dislocation loop algorithm developed by Dang *et al.*[26] (Disclaimer: the dimensions of the schematics are not scaled with the dimensions used in this work).

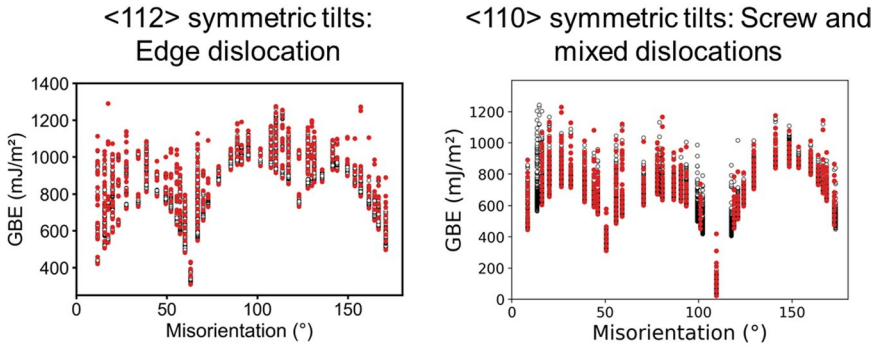

Fig. 3 Grain boundary energies for all 1000 possible (open circle) and chosen (solid red) grain boundary structures for <112> and <110> symmetric tilt grain boundary. Due to the infinitely long dislocation setup, the dislocation line has to be aligned with one of the dimensions. As a result, <112> STGB is used to study edge dislocation-GB interaction, while <110> STGB can be used to study screw and 60° mixed dislocation-GB interaction.

<110> STGBs, the simulation cell is approximately $1.0 \times 100.0 \times 48.0\ nm^3$ in the X, Y, and Z directions, respectively. Similarly, the simulation cell is approximately $1.8 \times 150.0 \times 80.0\ nm^3$ in the X, Y, and Z directions, respectively, for the <112> STGBs. This is to ensure that the boundary image force does not affect the results of the DGI. Due to varying boundary periodicity, different system sizes may be used for different grain boundary structures. The exact values of box sizes can be found in the GB data files.

To determine the structure of the tilt boundaries, different starting configurations are considered by translating grain 2 relative to grain 1, as shown in Fig. 2. The grain boundary region is defined as a 5 nm thick region across the Z direction (with the GB in the center), extending along the periodicity of X and Y directions. The grain boundary energy (GBE) is determined by normalizing the excess energy within the grain boundary region by the grain boundary area. Compared to previous studies where only minimum-energy structures are chosen, this dataset also considers DGI for high-energy metastable grain boundary structures. Figure 3 shows all chosen GB structures and their corresponding energies as a function of misorientation angles. For each misorientation angle, 1000 initial GB structures are generated. Among them, the ones with GB energies approximately 35 mJ/m^2 apart are chosen to evaluate interaction with dislocations. Although many GBs are considered in this work, it is now well known that grand canonical optimization strategies[32] may find structures missed by the standard γ-surface approach. Such structures could be computed to augment this dataset in the future.

Dislocation-grain boundary interactions. To model DGIs, an infinitely long edge dislocation dipole is generated in Grain 1 of < 112 > STGBs using a dislocation loop algorithm developed by Dang *et al.*[26,33]. This same approach is used to generate screw and mixed (60°) dislocation dipoles in Grain 1 of < 110 > STGBs. The dipole arm is approximately 36 nm to minimize interactions between individual dislocations. The chosen slip systems for the edge, screw, and mixed dislocations are $[\bar{1}10](11\bar{1})$, $[01\bar{1}](1\bar{1}\bar{1})$ and $[\bar{1}\bar{1}0](1\bar{1}\bar{1})$, respectively. Since the boundary is periodic in all three directions, there are two possible DGIs, of which only the interaction with the center GB is analyzed and reported. The dislocation dipole is positioned in a way that the right dislocation is approximately 10 nm away from the center of the GB region to minimize any short-range interactions initially. The system with the dislocation configuration is then equilibrated at 10 K via a Nosé-Hoover style thermostat and barostat[34]. To

Attribute	Value Datatype	Description	Notes
tx,ty,tz	Vector	GB tilt axis [h,k,l]	
nx,ny,nz	Vector	GB plane inclination [u,v,w]	
a,b,c	Vector	Indices of grid search over microscopic translational degrees of freedom	Grid spacing of d[h,k,l]/10 for a and b
d	Integer	Crystal chosen to delete atoms	
type	String	Dislocation type	Edge, screw, or mixed
Applied stress	Decimal	Applied stress (MPa)	
Misorientation angle	Decimal	Misorientation angle (degrees)	
Initial Velocity	Integer	Index of velocity seed	
GBE	Decimal	GB energy (mJ/m^2)	GB energy of the center grain where the interaction happens
Reaction	Integer	Dislocation-GB reaction label	See Table 2 for reaction categories

Table 1. Details of the attributes and values contained in the Dislocation-GB interaction dataset.

	Reaction
0	Undefined
1	Absorbed/Pinned
2	Partially transmitted
3	Fully transmitted
4	Reflected

Table 2. Dislocation-GB reaction labels.

Slip plane	Slip directions
(1,1,1)	[0,1, −1], [−1,0,1], [1, −1,0]
(1, −1, −1)	[0, −1,1], [−1,0, −1], [1,1,0]
(−1, −1,1)	[0, −1, −1], [1,0,1], [−1,1,0]
(−1,1, −1)	[0,1,1], [1,0, −1], [−1, −1,0]

Table 3. 12 slip systems for FCC materials considered for calculating the m' parameter. For each plane, there are three slip directions, resulting in 12 possible slip systems.

allow for comparison between different DGIs, a uniform stress state of pure resolved shear stress acting on the slip plane in the slip direction (pure Schmid stress) is applied in all cases[19]. Based on this local resolved shear stress, the macroscopically applied stress is determined for each DGI using a standard stress transformation operation. Three resolved shear stresses of 250, 500, and 750 MPa to glide the dislocation toward the GB are chosen to assess the effect of the driving force on the DGI. The DGI database also includes data for higher shear stress of 1 and 1.5 GPa for some <112> STGB where all DGI results are dislocation reflections from the GB at lower applied stress. Four different initial locations of the dislocation are also considered for <112> STGB. Moreover, the database also includes a subset of <110> STGBs where each interaction is repeated three times with different random initial atom velocities within a thermal distribution to determine if the results are statistically meaningful. The integration timestep in all simulations is 2 fs.

Geometrical criteria for DGI. To assist in the training of a future AI/ML model, m' values for all possible DGIs are also included. To compute m', the slip plane normal ($\vec{n}$) and slip direction ($\vec{d}$) are projected onto the respective grains using their orientation matrix. For example, $\bar{n}_g = \vec{n} \cdot g$ and $\bar{d}_g = \vec{d} \cdot g$.

$$m' = (\bar{n}_{g1} \cdot \bar{n}_{g2})(\bar{d}_{g1} \cdot \bar{d}_{g2}) \tag{1}$$

Here, $\bar{n}_{g1} \cdot \bar{n}_{g2}$ measures the angle between slip planes normals, and $\bar{d}_{g1} \cdot \bar{d}_{g2}$ the angle between slip directions. A m' of 1 suggests that the GB is transparent to dislocation, leading to effortless dislocation transmission, hence, no strengthening effect. A m' of 0 indicates no transmission across the GB but perhaps dislocation absorption or pinning at the GB. A negative value of m' highlights the different directions between slip plane normals and slip plane directions. The first step for calculating m' involves constructing the orientation matrix g for both grains. The symmetric tilt direction and GB plane are along the X and Y directions of the orientation matrix for the first grain (g_1, where dislocation is inserted), and their cross-product ($\vec{X} \times \vec{Y}$) is used to define

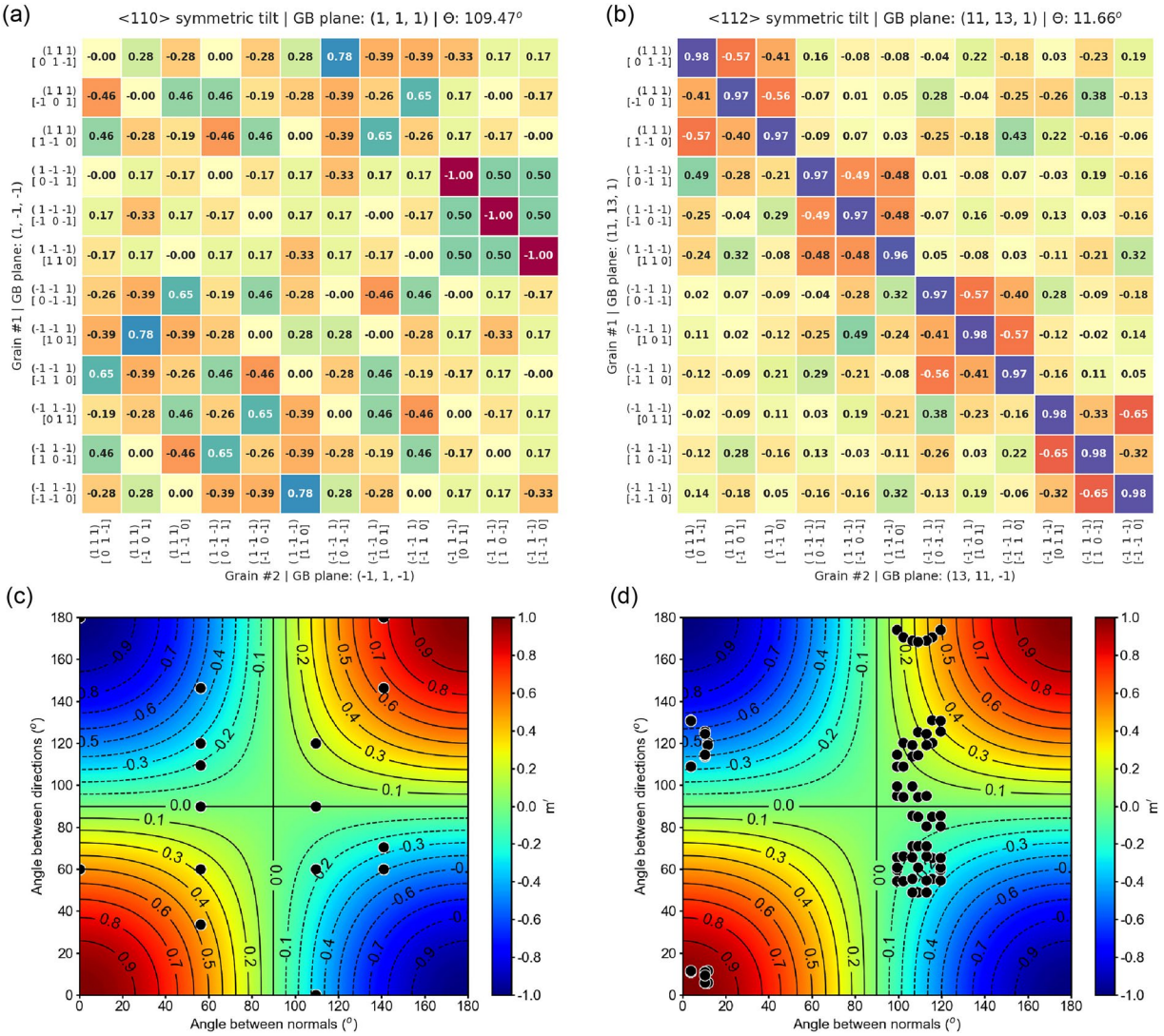

Fig. 4 Heatmaps showing the distribution of m' values across all possible slip systems for (**a**) <110> symmetric tilt grain boundary (GB) with a misorientation angle of 109.47° and (1,1,1) GB plane, and (**b**) <112> symmetric tilt GB with a misorientation angle of 11.66° and (11,13,1) GB plane. Panels (**c,d**) show contour plots of the m' values as functions of angular orientations of slip-plane normals and slip directions corresponding to cases (**a,b**), respectively. The background contour plots, using a jet colormap, illustrate the full range of possible m' values for FCC slip systems, covering angles from 0° to 180° for both slip directions and slip-plane normals. Black scatter points indicate the calculated m' values specific to the GB configurations presented in panels (**a,b**).

the Z-direction. The misorientation angle (Θ) is used to derive the orientation matrix for the second grain (g_2). The following are two examples for calculating the m' value for <110> and <112> symmetric tilts.

The misorientation angle, Θ, between g_1 and g_2 is calculated by constructing $\Delta g = g_2 \cdot g_1^{-1}$ and $\Theta = \cos^{-1}\left(\frac{Trace(\Delta g) - 1}{2}\right)$. The 12 slip systems mentioned in Table 3 are considered for calculating the m' parameter. These angles are used to plot the distribution showing possible m' values for slip transmission. For all 12 slip systems mentioned in Table 3, Eq. 1 gives 144 m' values. However, a note should be made that the stress in the first grain is applied in such a way that only one slip system is activated. Therefore, only 12 m' values would be of interest to examine the DGI based on the geometrical criteria. The database includes a total of 31 distinct <110> symmetric tilt grain boundaries that have different misorientation angles or (minimum energy structures) and similarly 42 distinct <112> symmetric tilt structures. Note that these values do not change for metastable boundaries. Hence, this highlights the importance of considering metastable GB structure for DGI. For each case, m' values for slip transmission are calculated for all 144 combinations and plotted as a heatmap, which can be found in the heatmap excel spreadsheets in the Materials Cloud Archive repository[35]. Figure 4 shows example for <110> symmetric tilt with (1,1,1) GB plane and <112> symmetric tilt with (11,13,1) GB plane.

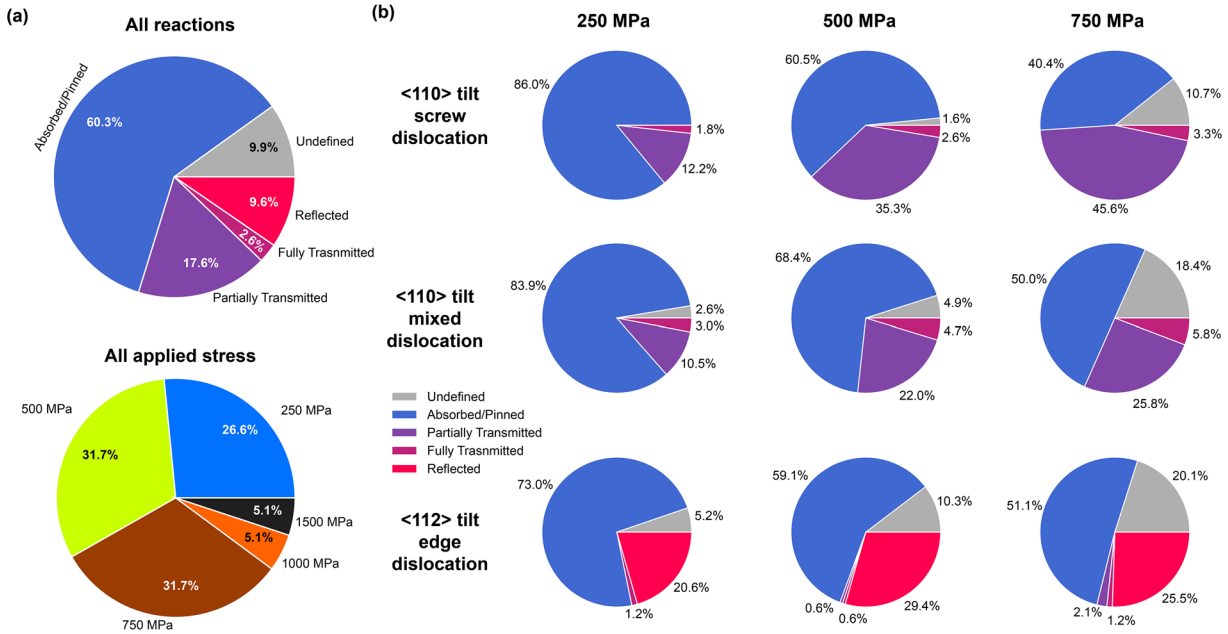

Fig. 5 Visualization of the DGI outcome database for <110> and <112>.

Data Records

The raw simulation data is not included in the database due to its inherently large size. Instead, the input files and the GB structures to reproduce these results are included in the template.zip file that can be retrieved from the Materials Cloud Archive repository[35]. Specifically, each misorientation contains subfolders of different GB structures whose folder name is their GB energy. For each GB structure, there are two folders named "screw" and "mixed" for screw and 60° mixed dislocations, respectively. Each of these folders contains LAMMPS input and data files to reproduce the dislocation-GB interactions. The dislocation-GB dataset of <110> and <112> STGBs in Cu is reported in DisGBDatabase.xlsx and can be retrieved from the Materials Cloud Archive repository[35]. The dataset contains 5234 unique dislocation-GB interaction entries (rows or data points). All the attributes (column headers) for these entries and their descriptions are listed in Table 1. The attributes 'tx,ty,tz' and 'nx,ny,nz' define the orientation of the GB tilt axis and plane normal, respectively. These values represent the macroscopic degree of freedom of the GB structure. Based on this, for each of the GB families, one can determine the 'misorientation angle' attribute. On the other hand, the attributes 'a,b,c' represents the indices of the grid search for the microscopic degrees of freedom for the local grain boundary structures. Attribute 'type' represents the type of incoming lattice dislocation. It can be either edge, screw, or 60° mixed dislocations. Attribute 'applied stress' indicates the Schmid applied stress (pure shear stress in the slip direction on the slip plane) to drive the dislocation toward the GB. Attribute 'GBE' details the GB energy corresponding to the center grain where the interaction happens. Finally, the attribute 'reaction' describes the outcome of the interaction. Based on simulation results manually analyzed via DXA in OVITO, the results are manually binned in one of the following outcomes: (1) dislocation reflection from the GB, (2) dislocation absorption/pinning at the GB, (3) dislocation partially transmitted through the GB when only leading partial can transmit and trailing partial is pinned at the GB, or (4) dislocation fully transmitted through the GB. The outcome of DGI can also be undefined if different outcomes occur simultaneously.

Technical Validation

Comparison with previous MD simulations. Figure 5 shows the summary of the DGI outcomes for this database. For edge dislocations, very few transmissions are observed, even at the applied stress of 750 MPa. Moreover, about 20 to 30% of edge dislocation was reflected/repelled from the GB. As the applied stress increased, more edge dislocations get absorbed into the <112> GB instead of repelling. For screw and mixed dislocation interactions with <110> tilt boundaries, the propensity to transmit (both partial and full transmission) increases with increasing applied shear stress. The results from this database show that the dislocation transmissibility generally follows: screw > mixed > edge.

Figure 6 plots the results of DGIs for different applied stress, dislocation types, misorientation angles, GB types, and GBE. From this plot, the transmission and repulsion cluster of data can be observed. This indicates that macroscopic factors such as the misorientation angles are important to DGI. Overall, higher misorientation angles make slip transmission more difficult, which was supported by many previous experimental results[5,36–38]. For the same misorientation angle, there are metastable GBs with different structures and corresponding GBEs whose reactions are different from each other[23]. Importantly, the effects are more evident for high applied shear stresses (500 and 750 MPa). Together, this indicates that microscopic parameters such as the GB local structures and dislocation types are also important to the outcomes of the DGIs.

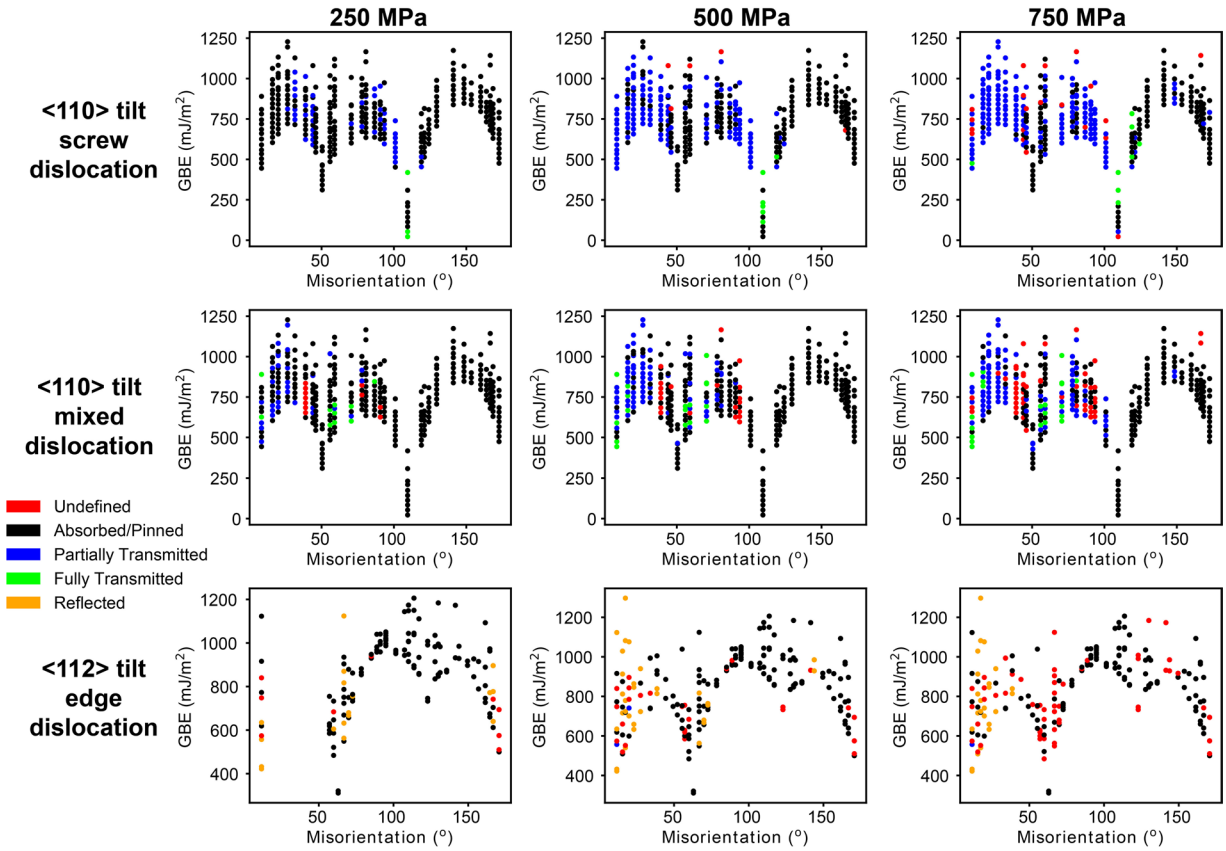

Fig. 6 DGI outcome database for different dislocation types, applied stress, misorientation angles, as well as <110> and<112> STGBs at fixed initial velocity and dislocation-GB interaction site. Each data point represents a dislocation-GB interaction where the color represents the outcome. Red is undefined results, orange is reflection of the dislocation from the GB, black is pinning and/or absorption of the dislocation into the GB, blue is transmission of the leading partial dislocation through the GB, and green is transmission of both leading and trailing dislocations through the GB.

To further validate the database, DGI results for two of the most well-studied grain boundaries were checked. They are the coherent and incoherent twin boundary (CTB and ITB, respectively) (misorientation angles of 70.5° and 109.5° as shown in Fig. 6, respectively) with simple structures and important role in deformation[29,30]. Indeed, our results show that the screw dislocation absorbs into the minimum-energy CTB similar to previous atomistic simulations using the same interatomic potentials[29,30] and experiments where the coherent TB can absorb the dislocation, thus providing resistance to slip transmission[30]. Furthermore, our variations in dislocation transmission and pinning when 60° mixed dislocations interact with ITB depending on the interaction sites are also consistent with previous MD simulations[39,40].

Interestingly, in Fig. 6, the first-row data indicate that for a 109° misorientation GB, screw dislocation transmission occurs at 250 MPa, but not at 500 MPa. These results demonstrated that the outcome of the dislocation-GB interaction for each interaction can be statistically varying. Indeed, for the case where transmission occurs at 250 MPa, the simulations were repeated twice with different initial sampling of the starting velocities. In both cases, the transmission does not occur, which is consistent with observation for higher stress at 500 and 750 MPa. These results further highlight the importance of including statistical variation in generating MD simulation dataset, which was done in this work.

Code availability

The input files and the GB structures to reproduce these results are included in the template.zip file that can be retrieved from the Materials Cloud Archive repository[35].

Received: 20 February 2025; Accepted: 19 May 2025;
Published online: 07 June 2025

References

1. Lu, K., Lu, L. & Suresh, S. Strengthening Materials by Engineering Coherent Internal Boundaries at the Nanoscale. *Science (1979)* **324**, 349–352, https://doi.org/10.1126/science.1159610 (2009).
2. Lin, Y., Pan, J., Zhou, H. F., Gao, H. J. & Li, Y. Mechanical properties and optimal grain size distribution profile of gradient grained nickel. *Acta Mater* **153**, 279–289, https://doi.org/10.1016/j.actamat.2018.04.065 (2018).

3. Zhu, Y. *et al*. Ultrastrong nanotwinned titanium alloys through additive manufacturing. *Nat Mater* **21**, 1258–1262, https://doi.org/10.1038/s41563-022-01359-2 (2022).
4. Liu, W. *et al*. Dislocation-grain boundary interaction in metallic materials: Competition between dislocation transmission and dislocation source activation. *J Mech Phys Solids* **145**, 104158, https://doi.org/10.1016/j.jmps.2020.104158 (2020).
5. Kacher, J., Eftink, B. P., Cui, B. & Robertson, I. M. Dislocation interactions with grain boundaries. *Curr Opin Solid State Mater Sci* **18**, 227–243, https://doi.org/10.1016/j.cossms.2014.05.004 (2014).
6. Javaid, F., Pouriayevali, H. & Durst, K. Dislocation–grain boundary interactions: recent advances on the underlying mechanisms studied via nanoindentation testing. *J Mater Res* **36**, 2545–2557, https://doi.org/10.1557/s43578-020-00096-z (2021).
7. Hansen, N. Hall–Petch relation and boundary strengthening. *Scr Mater* **51**, 801–806, https://doi.org/10.1016/j.scriptamat.2004.06.002 (2004).
8. Fensin, S. J., Cerreta, E. K., Gray, G. T. III & Valone, S. M. Why are some Interfaces in Materials Stronger than others? *Sci Rep* **4**, 5461, https://doi.org/10.1038/srep05461 (2014).
9. Vetterick, G. A. *et al*. Achieving Radiation Tolerance through Non-Equilibrium Grain Boundary Structures. *Sci Rep* **7**, 12275, https://doi.org/10.1038/s41598-017-12407-2 (2017).
10. El-Atwani, O. *et al*. Grain boundary metastability controls irradiation resistance in nanocrystalline metals (2024).
11. He, M., Wang, Y. & Fan, Y. Metastable grain boundaries: the roles of structural and chemical disorders in their energetics, non-equilibrium kinetic evolution, and mechanical behaviors. *Journal of Physics: Condensed Matter* **36**, 343001, https://doi.org/10.1088/1361-648X/ad4aab (2024).
12. Luster, J. & Morris, M. A. Compatibility of deformation in two-phase Ti-Al alloys: Dependence on microstructure and orientation relationships. *Metallurgical and Materials Transactions A* **26**, 1745–1756, https://doi.org/10.1007/BF02670762 (1995).
13. Cheng, Y., Mrovec, M. & Gumbsch, P. Atomistic simulations of interactions between the 1/2<111> edge dislocation and symmetric tilt grain boundaries in tungsten. *Philosophical Magazine* **88**, 547–560, https://doi.org/10.1080/14786430801894577 (2008).
14. Dewald, M. & Curtin, W. A. Multiscale modeling of dislocation/grain-boundary interactions: III. 60° dislocations impinging on Σ3, Σ9 and Σ11 tilt boundaries in Al. *Model Simul Mat Sci Eng* **19**, 055002, https://doi.org/10.1088/0965-0393/19/5/055002 (2011).
15. Bachurin, D. V., Weygand, D. & Gumbsch, P. Dislocation–grain boundary interaction in <111> textured thin metal films. *Acta Mater* **58**, 5232–5241, https://doi.org/10.1016/j.actamat.2010.05.037 (2010).
16. Ezaz, T., Sangid, M. D. & Sehitoglu, H. Energy barriers associated with slip–twin interactions. *Philosophical Magazine* **91**, 1464–1488, https://doi.org/10.1080/14786435.2010.541166 (2011).
17. Li, L., Liu, L. & Shibutani, Y. Defect interaction summary between edge dislocations and <112>-axis symmetric tilt grain boundaries in copper on activation barriers and critical stresses. *Int J Plast* **149**, 103153, https://doi.org/10.1016/j.ijplas.2021.103153 (2022).
18. Adams, D. W., Fullwood, D. T., Wagoner, R. H. & Homer, E. R. Atomistic survey of grain boundary-dislocation interactions in FCC nickel. *Comput Mater Sci* **164**, 171–185, https://doi.org/10.1016/j.commatsci.2019.04.007 (2019).
19. Suresh, S., Dang, K. & Fensin, S. J. Sensitivity of Dislocation-GB interactions to simulation setups in atomistic models. *Comput Mater Sci* **221**, 112085, https://doi.org/10.1016/j.commatsci.2023.112085 (2023).
20. Olmsted, D. L., Foiles, S. M. & Holm, E. A. Survey of computed grain boundary properties in face-centered cubic metals: I. Grain boundary energy. *Acta Mater* **57**, 3694–3703, https://doi.org/10.1016/j.actamat.2009.04.007 (2009).
21. Homer, E. R. *et al*. Examination of computed aluminum grain boundary structures and energies that span the 5D space of crystallographic character. *Acta Mater* **234**, 118006, https://doi.org/10.1016/j.actamat.2022.118006 (2022).
22. Tschopp, M. A., Coleman, S. P. & McDowell, D. L. Symmetric and asymmetric tilt grain boundary structure and energy in Cu and Al (and transferability to other fcc metals). *Integr Mater Manuf Innov* **4**, 176–189, https://doi.org/10.1186/s40192-015-0040-1 (2015).
23. Dang, K. *et al*. Interplay between dislocation type and local structure in dislocation-twin boundary reactions in Cu. *Phys Rev Mater* **8**, 063604, https://doi.org/10.1103/PhysRevMaterials.8.063604 (2024).
24. Page, D. E., Fullwood, D. T., Wagoner, R. H. & Homer, E. R. Atomistic simulations of incident dislocation interactions with nickel grain boundaries. *Model Simul Mat Sci Eng* **32**, 075006, https://doi.org/10.1088/1361-651X/ad6eab (2024).
25. Fensin, S. J., Asta, M. & Hoagland, R. G. Temperature dependence of the structure and shear response of a Σ11 asymmetric tilt grain boundary in copper from molecular-dynamics. *Philosophical Magazine* **92**, 4320–4333, https://doi.org/10.1080/14786435.2012.705911 (2012).
26. Dang, K., Capolungo, L. & Spearot, D. E. Nanoscale dislocation shear loops at static equilibrium and finite temperature. *Model Simul Mat Sci Eng* **25**, 085014, https://doi.org/10.1088/1361-651X/aa9390 (2017).
27. Thompson, A. P. *et al*. LAMMPS - a flexible simulation tool for particle-based materials modeling at the atomic, meso, and continuum scales. *Comput Phys Commun* **271**, 108171, https://doi.org/10.1016/j.cpc.2021.108171 (2022).
28. Mishin, Y., Mehl, M. J., Papaconstantopoulos, D. A., Voter, A. F. & Kress, J. D. Structural stability and lattice defects in copper: *Ab initio*, tight-binding, and embedded-atom calculations. *Phys Rev B* **63**, 224106, https://doi.org/10.1103/PhysRevB.63.224106 (2001).
29. Jin, Z.-H. *et al*. The interaction mechanism of screw dislocations with coherent twin boundaries in different face-centred cubic metals. *Scr Mater* **54**, 1163–1168, https://doi.org/10.1016/j.scriptamat.2005.11.072 (2006).
30. Chassagne, M., Legros, M. & Rodney, D. Atomic-scale simulation of screw dislocation/coherent twin boundary interaction in Al, Au, Cu and Ni. *Acta Mater* **59**, 1456–1463, https://doi.org/10.1016/j.actamat.2010.11.007 (2011).
31. Stukowski, A. Visualization and analysis of atomistic simulation data with OVITO–the Open Visualization Tool. *Model Simul Mat Sci Eng* **18**, 015012, https://doi.org/10.1088/0965-0393/18/1/015012 (2010).
32. Chen, E., Heo, T. W., Wood, B. C., Asta, M. & Frolov, T. Grand canonically optimized grain boundary phases in hexagonal close-packed titanium. *Nat Commun* **15**, 7049, https://doi.org/10.1038/s41467-024-51330-9 (2024).
33. Dang K., Bamney D., Bootsita K., Capolungo L. & Spearot D. E. Mobility of dislocations in Aluminum: Faceting and asymmetry during nanoscale dislocation shear loop expansion, *Acta Mater* **168**, https://doi.org/10.1016/j.actamat.2019.02.034 (2019).
34. Melchionna, S., Ciccotti, G. & Lee Holian, B. Hoover *NPT* dynamics for systems varying in shape and size. *Mol Phys* **78**, 533–544, https://doi.org/10.1080/00268979300100371 (1993).
35. Dang, K. *et al*. Dislocation-grain boundary interaction dataset for FCC Cu, (2025). https://archive.materialscloud.org/record/2025.65 (accessed May 26, 2025).
36. Livingston, J. D. & Chalmers, B. Multiple slip in bicrystal deformation. *Acta Metallurgica* **5**, 322–327, https://doi.org/10.1016/0001-6160(57)90044-5 (1957).
37. Shen, Z., Wagoner, R. H. & Clark, W. A. T. Dislocation and grain boundary interactions in metals. *Acta Metallurgica* **36**, 3231–3242, https://doi.org/10.1016/0001-6160(88)90058-2 (1988).
38. Lee, T. C., Robertson, I. M. & Birnbaum, H. K. Prediction of slip transfer mechanisms across grain boundaries. *Scripta Metallurgica* **23**, 799–803, https://doi.org/10.1016/0036-9748(89)90534-6 (1989).
39. Liang, Y. *et al*. Slip transmission for dislocations across incoherent twin boundary. *Scr Mater* **166**, 39–43, https://doi.org/10.1016/j.scriptamat.2019.02.042 (2019).
40. Ma, T. *et al*. Dislocation transmission across Σ3{112} incoherent twin boundary: a combined atomistic and phase-field study. *Acta Mater* **223**, 117447, https://doi.org/10.1016/j.actamat.2021.117447 (2022).

Acknowledgements
Research presented in this work was fully supported by the Laboratory Directed Research and Development program of Los Alamos National Laboratory, United States under Grant No. 20210036DR, "Investigating How Material's Interfaces and Dislocations Affect Strength" (iMIDAS). This research used resources provided by the Los Alamos National Laboratory Institutional Computing Program, which is supported by the U.S. Department of Energy National Nuclear Security Administration under Contract No. 89233218CNA000001.

Author contributions
S.F. conceived the project, K.D. and S.S. conceived the data acquisition process. K.D., S.S., A.M., I.C. oversaw and carried out the data extraction. All authors contributed to the database verification and writing the manuscript.

Competing interests
The authors declare no competing interests.

Additional information
Correspondence and requests for materials should be addressed to S.F.

Reprints and permissions information is available at www.nature.com/reprints.

Publisher's note Springer Nature remains neutral with regard to jurisdictional claims in published maps and institutional affiliations.